Exotic vector charmonium and its leptonic decay width [*]

Ying Chen(陈莹)[1,2;1)]   Wei-Feng Chiu(邱伟峰)[1,2]   Ming Gong(宫明）[1,2]   Long-Cheng Gui(桂龙成)[3,4]

Zhao-Feng Liu(刘朝峰)[1,2]

[1] Institute of High Energy Physics, Chinese Academy of Sciences, Beijing 100049, China
[2] Theoretical Center for Science Facilities, Chinese Academy of Sciences, Beijing 100049, China
[3] Department of Physics and Synergetic Innovation Center for Quantum Effects and Applications,
Hunan Normal University, Changsha 410081, China
[4] Key Laboratory of Low-Dimensional Quantum Structures and Quantum Control of Ministry of Education, Changsha 410081, China

Abstract: We propose a novel type of interpolating field operator, which manifests the hybrid-like configuration that the charm quark-antiquark pair recoils against gluonic degrees of freedom. A heavy vector charmonium-like state with a mass of $4.33(2)$ GeV is disentangled from the conventional charmonium states in the quenched approximation. This state has affinity for the hybrid-like operators but couples less to the relevant quark bilinear operator. We also try to extract its leptonic decay constant and give a tentative upper limit that it is less than one tenth of that of J/ψ, which corresponds to a leptonic decay width about dozens of eV. The connection of this state with X(4260) is also discussed.

1   Introduction

X(4260) has been observed by many experiments as a $\pi\pi J/\psi$ resonance structure in the initial state radiation (ISR) process $e^+e^- \to \gamma_{\mathrm{ISR}} J/\psi \pi\pi$ [1–3]. Its resonance parameters are determined now to be $M_{\mathrm{X}} = 4251(9)$ MeV and $\Gamma_{\mathrm{X}} = 120(12)$ MeV [4]. Based on its production mode, X(4260) must have the quantum number $J^{\mathrm{PC}} = 1^{--}$. In addition, the ratio of X(4260) $\to$ $\pi^+\pi^- J/\psi$ and X(4260) $\to \pi^0\pi^0 J/\psi$ events observed by the CLEO collaboration is consistent with X(4260) being an isoscalar. In other words, X(4260) has the same quantum number as that of the vector charmonia J/ψ, ψ', etc. However, in contrast to the ψ states, X(4260) has not yet been observed directly in e^+e^- annihilation. On the other hand, its mass is well above the $D\bar{D}$ threshold, but it has been observed only in the $J/\psi\pi^+\pi^-$ system instead of the $D\bar{D}$ ones. These facts may imply that X(4260) has a large branching fraction for the $J/\psi\pi^+\pi^-$ decay mode. Thus, the small combined width $\Gamma(\mathrm{X} \to e^+e^-)Br(\mathrm{X} \to J/\psi\pi\pi) = 9.2 \pm 1.0\,\mathrm{eV}$ can be understood as $X(4260)$ having a very small e^+e^- width.

These features motivate conjectures that X(4260) might be an exotic state, for example, a hybrid charmonium [5–7]. More theoretical information for X(4260) is needed in order to unravel its nature, among which the leptonic decay width of X(4260) is an important quantity.

As far as hybrid charmonium is concerned, extensive lattice QCD studies have been devoted to the $J^{\mathrm{PC}} = 1^{-+}$ channel. In the constituent quark model picture, this quantum number cannot appear in the $q\bar{q}$ system, therefore it is usually conjectured that additional degrees of freedom should be involved and the minimum configuration can be $q\bar{q}g$ where g is a constituent gluon. The corresponding $q\bar{q}g$ interpolation fields are used in lattice calculations which predict the mass of the 1^{-+} charmonium-like state to be around 4.3 GeV [8–17]. Similar studies have been also extended to investigate possible hybrids with the conventional quantum number, but the challenging task is to distinguish these states from conventional mesons. The state-of-the-art approach for this goal is the variational method based on large enough operator sets built through sophisticated methods. In the vector channel, there is a state observed with a

mass round 4.4 GeV [14], which couples weakly to the quark bilinear operator but seems closely coupled with quark-antiquark-gluon operators.

Generally speaking, the appearance of an interpolating field operator does not necessarily reflect the inner structure of a hadron state. However, for heavy quark systems where the non-relativistic picture may be available to some extent, the coupling of the operator to a specific state may bear some useful information about its status. Taking a mesonic hybrid, for example, even though it is an ambiguous concept from the point of view of quantum chromodynamics (QCD), it is always thought of as a hadron state made up of a quark-antiquark pair plus a constituent gluonic component in the constituent quark model picture. Of course one can also relax the definition of a hybrid to an exotic object which has an additional degree of freedom apart from the constituent quarks. This kind of additional degree of freedom can be a fluctuating flux tube in the flux tube model, the color bag of the MIT bag model, etc. There is also a recent study on quarkonium hybrids using non-relativistic effective field theory [18]. The essence of the exotic nature of a meson state is that the constituent $q\bar{q}$ pair acquires a center-of-mass motion by recoiling against the additional degrees of freedom, which is distinct from the conventional hadron states. This is our starting point to build a novel type of hybrid-like operator. We split the charm quark-antiquark pair component and the gluon field in the $q\bar{q}g$ operator into two parts with different spatial separations. In momentum space, this manifests the center-of-mass motion of $q\bar{q}$ pair in the rest frame of the state. We calculate the correlation functions of these operators, from which we try to extract the possible exotic charmonium state. Since the operators with different spatial separations provide different correlation functions, we fit them simultaneously along with the correlation function involving the electromagnetic current to obtain the decay constants of the states which contribute significantly.

This paper is organized as follows. Section 2 contains a description of the construction of the new lattice interpolation operators for the hybrid-like vector meson. The lattice parameters and the numerical techniques are presented in Section 3. We discuss our results and their connections with X(4260) in Section 4. The conclusions and a summary can be found in Section 5.

2   New interpolation field for exotic vector charmonium

We focus on the exotic vector charmonium ($J^{PC} = 1^{--}$) by assuming a hybrid-like configuration $c\bar{c}g$. A simple and straightforward local operator possibly reflecting this constituent configuration is $O_i^{(H)}(x) =$ $\bar{c}^a(x)\gamma_5 c^b(x)B_i^{ab}(x)$, where a,b are color indices, i the spatial index, and $B_i^{ab}(x) = \frac{1}{2}\epsilon_{ijk}F_{jk}^{ab}$ the chromomagnetic field tensor. This kind of operator can be compared with the commonly used quark bilinear operator for the vector $O_i^{(M)} = \bar{c}\gamma_i c(x)$. In order to find the non-relativistic form of these interpolation operators, we use the Foldy-Wouthuysen-Tani transformation [19] to decompose the charm quark and antiquark fields (Dirac spinor) in terms of the Pauli spinors $\phi/\phi^\dagger$ which annihilates/creates a charm quark, and $\chi/\chi^\dagger$ which creates/annihilates a charm antiquark. The explicit expressions of the operators $O_i^{(H)}(x)$ and $O_i^{(M)}$ to the lowest order of the nonrelativistic approximation can be written as

$$O_i^{(H)} \equiv \bar{c}^a\gamma_5 c^b B_i^{ab} \rightarrow \chi^{a\dagger}\phi^b B_i^{ab} + O\left(\frac{1}{m_c}\right),$$

$$O_i^{(M)} \equiv \bar{c}^a\gamma_i c^a \rightarrow \chi^{a\dagger}\sigma_i\phi^a + O\left(\frac{1}{m_c}\right), \quad (1)$$

where one can see that the block $\chi^{a\dagger}\phi^b$ of the $O_i^{(H)}$ operator is a spin singlet and color octet, while that of $O_i^{(M)}$ is a spin triplet and color singlet. Intuitively $O_i^{(H)}$ couples more to a state of spin singlet charm quark-antiquark pair and less to a state of spin triplet $\bar{c}c$ component owing to the heavy quark mass suppression for the spin flipping of a heavy quark, and vice versa for $O_i^{(M)}$. In order to resemble the center-of-mass motion of the $c\bar{c}$ recoiling against an additional degree of freedom, we split the operator $O_i^{(H)}$ into two spatial parts, $\bar{c}^a\gamma_5 c^b$ and B_i^{ab}, separated by an explicit spatial displacement $\boldsymbol{r}$. In a fixed gauge (the Coulomb gauge in this work), we get a set of spatially extended operators,

$$O_i^{(H)}(\boldsymbol{x},t;\boldsymbol{r}) = (\bar{c}^a\gamma_5 c^b)(\boldsymbol{x},t)B_i^{ab}(\boldsymbol{x}+\boldsymbol{r},t). \quad (2)$$

It is expected that the coupling of this type of operator to the conventional charmonia (without the center-of-mass motion of charm quark-antiquark pair in the non-relativistic picture) would be suppressed, while the coupling to the exotic state can be enhanced.

3   Numerical details

We use the tadpole-improved gauge action [20–22] to generate gauge configurations on anisotropic lattices with the temporal lattice spacing much finer than the spatial one. The aspect ratio takes $\xi = a_s/a_t = 5$, where a_s and a_t are the spatial and temporal lattice spacing, respectively. Two lattices $L^3 \times T = 8^3 \times 96(\beta = 2.4)$ and $12^3 \times 144(\beta = 2.8)$ with different lattice spacings are used to check the discretization artifacts and the relevant input parameters are listed in Table 1, where a_s values are determined from $r_0^{-1} = 410(20)$ MeV. We use the tadpole-improved clover action to calculate the quark propagators. The relevant parameters

in the fermion action are tuned carefully by requiring that the physical dispersion relations of vector and pseudoscalar mesons are correctly reproduced at each bare quark mass [23, 24]. The bare charm quark masses at different β are determined from the physical mass of J/ψ, $m_{J/\psi} = 3.097$ GeV. The spatial extension of both lattices is ~ 1.7 fm, which is tested to be large enough for charmonium states. The ground state masses of $1S$ and $1P$ charmonia calculated on these two lattices (see Fig. 2 and Table II of Ref. [25] for the details) show that the finite a_s effects are small. Since the spatial extended interpolation operators $O_i^{(H)}$ discussed above are gauge variant, we carry out the calculation of the quark propagators and correlation functions after transforming each configuration to the Coulomb gauge.

Table 1.   The input parameters for the calculation. Values of the coupling β, anisotropy ξ, the lattice size, and the number of measurements are listed. a_s/r_0 is determined by the static potential, the first error of a_s is the statistical error and the second one comes from the uncertainty of the scale parameter $r_0^{-1} = 410(20)$ MeV.

β	ξ	a_s	La_s/fm	$L^3 \times T$	N_{conf}
2.4	5	0.222(2)(11)	~ 1.78	$8^3 \times 96$	1000
2.8	5	0.138(1)(7)	~ 1.66	$12^3 \times 144$	1000

3.1   Data analysis strategy

Our first task is to verify the existence of the exotic vector charmonium. We use the following source operator to calculate the correlation functions,

$$O_i^{(W)}(\tau) = \sum_{\boldsymbol{y},\boldsymbol{z}} \bar{c}^a(\boldsymbol{y},\tau)\gamma_5 B_i^{ab}(\boldsymbol{z},\tau)c^b(\boldsymbol{z},\tau), \qquad (3)$$

where τ refers to the source time slice. For the sink operator $O_i^{(H)}$, the two-point functions we calculate are

$$C^{(H)}(\boldsymbol{r},t;\tau) = \frac{1}{3}\sum_{\boldsymbol{x},i}\langle 0|O_i^{(H)}(\boldsymbol{x},t;\boldsymbol{r})O_i^{(W)\dagger}(\tau)|0\rangle$$

$$= \frac{1}{3}\sum_{\boldsymbol{x},\boldsymbol{y},\boldsymbol{z},i}\text{Tr}\,\big\langle S_F^\dagger(\boldsymbol{x},t;\boldsymbol{y},\tau)B_i(\boldsymbol{x}+\boldsymbol{r},t)$$

$$\times S_F(\boldsymbol{x},t;\boldsymbol{z},\tau)B_i^\dagger(\boldsymbol{z},\tau)\big\rangle, \qquad (4)$$

where $S_F(x,y)$ stands for the charm quark propagator. Accordingly, there are two types of wall-source quark propagators to be calculated. One of them uses the usual wall source by setting the source element to unity at each spatial site of the source time slice. The other one uses the source by multiplying the chromomagnetic field tensor $B_i(\boldsymbol{z},\tau)$ to each site of the plain wall source. In order to increase the statistics additionally, for each configuration we calculate T charm quark propagators

$S_F(\vec{x},t;\vec{0},\tau)$ by setting the corresponding source vectors on each time slice τ. This permits us to average over the temporal direction when calculating the two-point functions.

In practice, the two-point functions $C^{(H)}(\boldsymbol{r},t;\tau)$ with the same $r = |\boldsymbol{r}|$ are averaged, such that the quantum number is kept to be exactly $J^{PC} = 1^{--}$. After averaging over the time direction, the practical two-point functions we calculate are

$$C^{(H)}(r,t) = \frac{1}{TN_r}\sum_{|\boldsymbol{r}|=r}\sum_{\tau=1}^{T}C^{(H)}(\boldsymbol{r},t+\tau;\tau)$$

$$= \sum_i \Phi_i(r)\text{e}^{-m_i t}, \qquad (5)$$

where N_r is the degenerate degree of $r = |\boldsymbol{r}|$. In the data analysis stage, we perform a simultaneous multi-exponential fit to $C^{(H)}(r,t)$'s by using a correlated minimal-χ^2 fit method with the jackknife covariance matrix (we use three mass terms throughout this work).
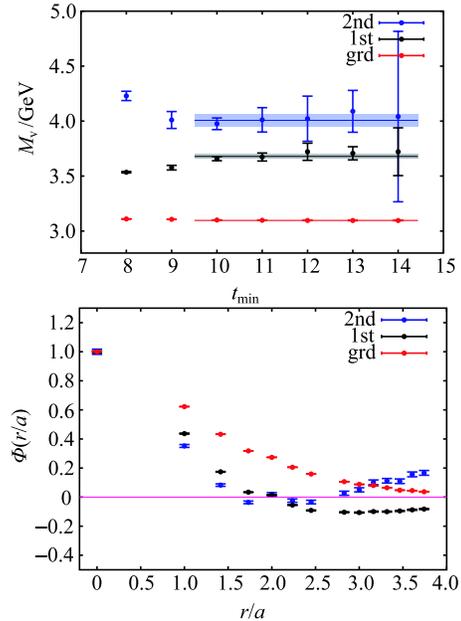
Fig. 1.   (color online) Upper panel: Masses of the three lowest states fitted to $C^{(M)}(r,t)$ with different t_{min} ($\beta = 2.4$). We average the masses in this range with each value weighted by its error and get the values $m_1 = 3.097(1)$ GeV, $m_2 = 3.679(19)$ GeV, and $m_3 = 4.007(57)$ GeV, respectively. Lower panel: $\Phi_i'(r/a)$'s (normalized as $\Phi_i'(0) = 1$) of the lowest three states. It is clearly seen that the nodal behaviors are very different for different states.

3.2   Masses and Bethe-Salpeter amplitudes of conventional vector charmonia

In order to test the reliability of the fitting strategy mentioned above, we first carry out a similar analysis to

the correlation functions $C^{(M)}(r,t)$ of the spatially extended version of operator $O^{(M)}$ on the $\beta = 2.4$ lattice. The procedure is detailed as follows. The spatially extended version of $O^{(M)}$ is defined as

$$O_i^{(M)}(\boldsymbol{x},t;\boldsymbol{r}) = \bar{c}(\boldsymbol{x},\tau)\gamma_i c(\boldsymbol{x}+\boldsymbol{r},\tau), \qquad (6)$$

whose correlation function with the corresponding wall source operator

$$O_i^{'(W)}(\tau) = \sum_{\boldsymbol{y},\boldsymbol{z}} \bar{c}(\boldsymbol{y},\tau)\gamma_i c(\boldsymbol{z},\tau), \qquad (7)$$

say, $C^{'(M)}(\boldsymbol{r},t+\tau;\tau)$, is defined similarly as in Eq. (4). After averaging over the temporal direction, we have

$$\begin{aligned} C^{'(M)}(r,t) &= \frac{1}{TN_r} \sum_{|\boldsymbol{r}|=r} \sum_{\tau=1}^{T} C^{'(M)}(\boldsymbol{r},t+\tau;\tau) \\ &= \sum_i \Phi_i'(r)\mathrm{e}^{-m_i t} \end{aligned} \qquad (8)$$

where $\Phi_i'(r)$ is the r-dependent spectral weight of the i-th state.

In the fitting procedure, we fix a maximal t (denoted by $t_{\max}$) and vary the lower bound $t_{\min}$ of the fit window, and find that the masses of the lowest three states keep constant to some extent for a series of $t_{\min}$, as shown in the upper panel of Figure 1. We average the masses in this range with each value weighted by its error and get the values $m_1 = 3.097(1)$ GeV, $m_2 = 3.679(19)$ GeV, and $m_3 = 4.007(57)$ GeV, respectively. These three states may correspond to J/ψ, ψ'(3686), and ψ(4040) and we can almost reproduce their experimental spectrum. We also plot the $\Phi_i'(r/a_\mathrm{s})$'s (normalized as $\Phi_i'(0) = 1$) in the bottom panel of Fig. 1, where one can find that there is no radial node for $\Phi_1'(r/a)$, one radial node for $\Phi_2'(r/a_\mathrm{s})$, and two radial nodes for $\Phi_3'(r/a_\mathrm{s})$. Given the quark model assignments n^3S_1 state for J/ψ, ψ(3686), and ψ(4040) with $n = 1,2,3$, respectively, this is actually not surprising, since $\Phi_i'(r)$ is proportional to the Coulomb Bethe-Salpeter amplitude of the i-th S-wave charmonium, which, at the leading order of the non-relativistic approximation, corresponds to the radial wave functions in the quark model [26, 27].

3.3   Existence of an exotic vector charmonia and its mass

From the above one can see that our data analysis strategy is robust for the conventional vector charmonium states, therefore we perform a similar study for the correlation functions described in Eq. (4) and (5).

Figure 2 shows the plots of $\Phi_i(r)$ with respect to r (in physical units) through a three-mass-term fit (the upper panel is for $\beta = 2.4$ at $t_{\min} = 12a_\mathrm{t}$, and the lower panel for $\beta = 2.8$), whose masses are fitted to be 3.100(7)

GeV, 3.58(9) GeV, and 4.6(2) GeV for $\beta = 2.4$, and 3.090(6) GeV, 3.54(5) GeV, and 4.6(1) GeV for $\beta = 2.8$ at $t_{\min} = 16a_\mathrm{t}$. $\Phi_1(r)$ and $\Phi_2(r)$ damp more rapidly and are close to zero near $r \sim 0.3$ fm while $\Phi_3(r)$ is still relatively large. The lowest two states very possibly correspond to the conventional vector charmonia J/ψ and ψ' according to their masses. In contrast, the third state, with a much higher mass, still dominates the two point functions with r larger than 0.3 fm. This may signal the exotic nature of this state that is reflected by the spatially extended sink operator $O_i^{(H)}$. Of course, the higher conventional vector charmonia, such as ψ(4040) and ψ(4415), should also contribute to the two-point function $C^{(H)}(r,t)$, however in our data analysis procedure, $C^{(H)}(r,t)$ cannot accommodate more statistically meaningful states. The presence of the higher conventional charmonia may result in a small shift of the masses of the fitted states. For example, the mass of the second state deviates from that of the would-be ψ' state.
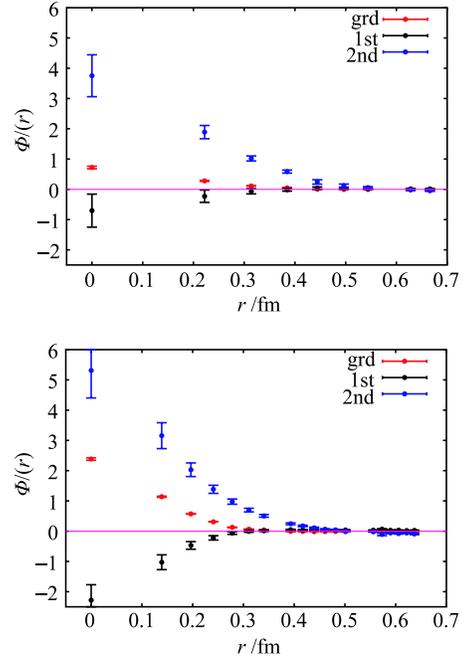
Fig. 2.   (color online) Plots of $\Phi_i(r)$ with respect to r (in physical units) for the three lowest states (the upper panel is for the $\beta = 2.4$ case, and the lower panel for $\beta = 2.8$).

It is seen from Fig. 2 that the r-behaviors of the first (J/ψ) and the second state (ψ') are similar up to an overall factor. If this is the case for all the conventional charmonium states, since the r behavior may depict the center-of-mass motion of the c̄c component and the conventional charmonia are free of this in the nonrelativistic approximation, we can conjecture that the spectral weights of the i-th conventional charmonia $\Phi_i(r)$ can be

factorized into $\Phi(r)W_i$ where $\Phi(r)$ is approximately uniform and insensitive to the different conventional charmonia, such that the two-point functions $C^{(H)}(r,t)$ with different r can be linearly combined to eliminate the contribution from the conventional charmonium states. In practice, we linearly combine the correlation functions $C^{(H)}(r,t)$ at two specific r_1 and r_2 as

$$C(\omega,t) = C^{(H)}(r_1,t) - \omega C^{(H)}(r_2,t), \qquad (9)$$

where ω is a tunable parameter. For each lattice, an optimal ω can be obtained by the requirement that the effective mass plateau of $C(\omega,t)$ is as long as possible. To be specific, for $\beta = 2.4$, we use $r_1 = 0$ and $r_2 = a_s$ and set $\omega = 2.576$, which is very close to the central value of the ratio $\Phi_1(0)/\Phi_1(a_s) = 2.583$ through the three-mass fit illustrated in Fig. 2. Using this omega and the fit results in Fig. 2, the spectral weights of the three states in $C(\omega,t)$ are roughly 0.002, -0.1, and -1.1, respectively. This implies that the relative contribution of the third state is strongly enhanced by this subtraction scheme. Similarly, for $\beta = 2.8$ we use $r_1 = a_s$ and $r_2 = \sqrt{3}a_s$ and set $\omega = 3.658$ which is also close to the central value of the ratio $\Phi_1(a_s)/\Phi_1(\sqrt{3}a_s) = 3.681$. The spectral weights of the three states are roughly 0.007, -0.2 and -1.9, respectively. In Fig. 3 we plot the effective mass plateaus of $C(\omega,t)$'s for $\beta = 2.4$ and $\beta = 2.8$. The t and the masses are expressed in physical units according to the lattice spacings listed in Table 1. One can see that both plateaus are fairly good and lie on top of each other. Since both the sink operator $O^{(H)}(r)$ and the source operator $O^{(W)}$ (whose correlation functions are $C^{(H)}(r,t)$) are expected to couple strongly to hybrid-like states and the contribution from the conventional charmonia is subtracted largely by the above scheme, we take the state reflected by the observed plateau as the exotic vector charmonium and name it X in the rest part of this work (we keep the name of the experimental state X(4260)). The horizontal line shows the fitted mass $M_X = 4.33(2)$ GeV through a one-exponential fit in the time range from 0.3 to 0.9 fm.
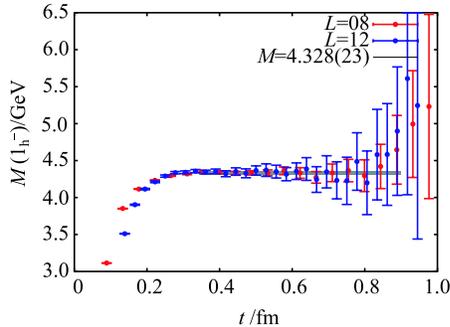

Fig. 3.   (color noline) The effective mass plateaus of $C(\omega,t)$'s for $\beta = 2.4$ (red points) and $\beta = 2.8$ (blue points). The horizontal line shows the fitted mass $M_X = 4.33(2)$ GeV through a one-exponential fit.

To this end, we claim that a vector charmonium-like state with a mass of 4.33(2) GeV has been unambiguously singled out, whose exotic nature may be reflected by its distinct coupling to the special interpolation field $O^{(H)}(r,t)$ in comparison with the conventional vector charmonia. It should be noted that this state has also been observed by previous lattice studies using variational methods based on lattice operator sets [14]. However, the spatially extended operators $O^{(H)}(r,t)$ we use give a clearer picture of its inner structure.

3.4   Leptonic decay constant of the exotic vector charmonium

Since this hybrid-like charmonium can be disentangled from the conventional charmonia with the prescription above, its leptonic decay constant can be investigated accordingly. The leptonic decay constant f_V of a vector meson state V is defined by

$$\langle 0|J_\mu^{(em)}(0)|V(\vec{p},r)\rangle = m_V f_V \epsilon_\mu(\vec{p},r), \qquad (10)$$

where $J_\mu^{(em)}(0)$ is the electromagnetic current and $\epsilon_\mu(\vec{p},r)$ is the polarization vector of V at momentum $\vec{p}$. For vector charmonium states, $J_\mu^{(em)}(0)$ can be approximated by $\bar{c}\gamma_\mu c(0)$ if the contribution from other quark flavors through annihilation diagrams is neglected. Since the vector current $J_\mu^{em}(x)$ defined in the continuum limit is no longer conserved on the lattice, we perform a nonperturbative renormalization procedure [28] to extract the multiplicative renormalization constant Z_V of the current. The renormalization constant of the spatial componets of J_μ^{em} is determined to be $Z_V^{(s)} = 1.39(2)$ for $\beta = 2.4$ and $Z_V^{(s)} = 1.11(1)$ for $\beta = 2.8$ [29].

Since the spatial components of $J_\mu^{(em)}(x)$ is exactly the normal quark bilinear operator $O_i^{(M)}$ for vector mesons, the matrix elements in Eq. (10) can be derived from the corresponding correlation functions involving the operator $O_i^{(M)}$ along with the vector current renormalization constant $Z_V^{(s)}$. In order to obtain this matrix elements, we also calculate two other categories of correlation functions in addition to $C^{(H)}(\boldsymbol{r},t)$,

$$C^{(J)}(t) = \frac{1}{3}\sum_{\boldsymbol{x},i}\langle 0|J_i(\boldsymbol{x},t)O_i^{(W)\,\dagger}(0)|0\rangle$$

$$C^{(W)}(t) = \frac{1}{3}\sum_i\langle 0|O_i^{(W)}(t)O_i^{(W)\,\dagger}(0)|0\rangle. \qquad (11)$$

where averaging over the temporal direction is also taken implicitly in the above expressions. After the intermediate states insertion to $C^{(J)}(t)$, $C^{(H)}(\boldsymbol{r},t)$, and $C^{(W)}(t)$, we have

$$C^{(J)}(t) = \sum_{n,r}\frac{1}{2m_n}Z_n^{(J)}Z_n^{(W)*}e^{-m_n t},$$

$$C^{(H)}(\boldsymbol{r},t) = \sum_{n,r} \frac{1}{2m_n} Z_n^{(H)}(r) Z_n^{(W)*} e^{-m_n t},$$

$$C^{(W)}(t) = \sum_{n,r} \frac{1}{2m_n V_3} Z_n^{(W)} Z_n^{(W)*} e^{-m_n t}, \qquad (12)$$

where m_n is the mass of the n-th state and the parameter $Z_n^{(K)}$ with K referring to H or W is defined as

$$\langle 0 | O_i^{(K)} | V_n(\boldsymbol{p},r) \rangle = Z_n^{(K)} \epsilon_i(\boldsymbol{p},r). \qquad (13)$$

Accordingly the leptonic decay constant f_{V_n} can be derived from $Z_n^{(J)}$ from the definition Eq. (10) as

$$f_{V_n} = C Z_V^{(s)} Z_n^{(J)} / m_n, \qquad (14)$$

where C is an overall constant prefactor owing to the redefinition of our quark fields and the anisotropic lattices we are using.

The time dependence of the correlation functions is usually observed from their effective mass plots. The effective masses of different correlation functions $C^{(X)}(t)$ are defined as

$$M_{\mathrm{eff}}(t)a = \log \frac{C^{(K)}(t)}{C^{(K)}(t+1)}, \qquad (15)$$

where K stands for J, H and W. These effective masses are illustrated in Fig. 4, where the mass of the ground state (J/ψ) is also plotted as a horizontal dashed line to guide the eye. The left panel of Fig. 4 is for the $\beta = 2.4$ lattice, and the right panel is for $\beta = 2.8$. In the plots, we present in the third row the effective mass of $C^{(H)}(r,t)$ at a specific r ($r = \sqrt{6}a_s$ for $\beta = 2.4$ and $r = 3a_s$, respectively), where $C^{(H)}(r,t)$ is dominated by the third state in the short time range, changes sign and is finally saturated by the ground state when t increases. This is manifested in the effective mass plot by the phenomenon that $M_{\mathrm{eff}}(t)$ shows a meta-stable plateau (roughly 4.4 GeV) higher than the ground state before the discontinuity time, and then converges to the mass of the ground state. This phenomenon also implies that the spectral weight of the third state is much larger than that of the lower states and the signs of the two spectral weights are different. In the fitting procedure, we fix the maximal time $t_{\max}$ of the fitting window ($t_{\max} = 30a_t$ for $\beta = 2.4$ and $t_{\max} = 40a_t$ for $\beta = 2.8$), and let the minimal time vary over a range. The fitted spectral weights of $C^{(J)}(t)$ and $C^{(W)}(t)$ are listed in Table 2 (raw data), from which the decay constants can be derived. The fitted masses and the decay constants are converted to the values in physical units (GeV) and are presented in Table 3. The spectral weights of $C^{(H)}(r,t)$ are less relevant and omitted here to save space (one can refer to Fig. 2 to see their relative magnitudes for the three states). All the errors are statistical and obtained through a jackknife analysis. In order to illustrate the fit

quality, we also show the effective masses (in blue bands) of the functions in Eq. (12) using the fitted parameters at $t_{\min} = 12a_t$ for $\beta = 2.4$ and $t_{\min} = 16a_t$ for $\beta = 2.8$. The fit functions describe the measured data very well. For all the fits, the $\chi^2/N_{\mathrm{d.o.f}}$'s are around 1 even though the number of degrees-of-freedom $N_{\mathrm{d.o.f}}$ is always several hundreds.

As shown in Table 2 and Table 3, the fitted parameters are almost stable and insensitive to $t_{\min}$. The masses of the first and the second states are consistent with the those of J/ψ and ψ', while the mass of the third state is a little higher than the hybrid-like state we obtained before. This can be attributed to some extent to contamination from even higher states. In the right part of Table 2, the spectral weights $|Z_3^{(W)}|^2$ are an order of magnitude larger than those of the lowest two states (corresponding mostly to J/ψ and ψ'). This is not strange since $Z_n^{(W)}$ is the coupling of the hybrid-like wall-source operator $O^{(W)}$ to the n-th state and is expected to be enhanced when coupling to a hybrid-like state. In contrast, the spectral weights $|Z_n^{(J)} Z_n^{(W)}|$ (in the left part of Table 2) of the lowest two states, even suppressed by $Z_n^{(W)}$, are much larger than that of the third state which are close to zero with errors. This may imply that the decay constant of the third state is very small, since $Z_n^{(J)}$ is proportional to the decay constant of the n-th state. Using the fitted spectral weights $Z_n^{(J)} Z_n^{(W)}$ and $|Z_n^{(W)}|^2$, we can get the concrete values of $Z_n^{(J)}$, from which the decay constant of the n-th state can be derived using Eq. (14). The derived decay constants of the three states are also listed in Table 3, where the last row lists the experimental values for comparison. For J/ψ, we get its decay constant to be roughly 0.46(2) GeV at $\beta = 2.4$ and 0.43(2)GeV at $\beta = 2.8$, which is close to the experimental value although 5%–10% larger. The deviation can be attributed to the artifact of the finite lattice spacings (and also the uncertainty owing to the quenched approximation). The derived decay constant of ψ', $f_{\psi'}$, seems compatible with the experimental value, but with huge errors which come mainly from the uncertainty of $|Z_2^{(W)}|^2$.

The most striking observation is that the decay constant f_3 of the third state is consistent with zero within the error. Superficially, it seems that the exotic vector charmonium has a nearly zero decay constant. However, there is a possibility that this is a mixing effect of two nearby states (for example, the would-be exotic state and $\psi(4415)$), whose contributions to $C^{(J)}(t)$ cancel to some extent, because we perform the simultaneous fit using only three mass terms. We have addressed that an exotic vector charmonium state does exist and contributes substantially to the correlation functions $C^{(H)}(r,t)$ in the previous subsection. This is also the case for $C^{(W)}(t)$ since $|Z_3^{(W)}|^2$ is one magnitude or even more larger than

$|Z_1^{(W)}|^2$ and $|Z_2^{(W)}|^2$. Based on these facts and considering the possible admixture of a conventional charmonium state to the exotic state, we try to estimate the upper limit of the decay constant of the exotic vector charmonium. If the third state is actually contributed from the would-be exotic state X and the adjacent vector charmonium state $\psi(4415)$, then the spectral weight $Z_3^{(J)}Z_3^{(W)}$ can be expressed as

$$Z_3^{(J)} Z_3^{(W)} = Z_X^{(J)} Z_X^{(W)} + Z_{\psi(4415)}^{(J)} Z_{\psi(4415)}^{(W)} \sim 0. \qquad (16)$$

Thus we have

$$|Z_X^{(J)}| \sim \frac{|Z_{\psi(4415)}^{(W)}|}{|Z_X^{(W)}|} |Z_{\psi(4415)}^{(J)}|. \qquad (17)$$

According to Eq. (14), this is equivalent to

$$f_X \sim \frac{|Z_{\psi(4415)}^{(W)}|}{|Z_X^{(W)}|} f_{\psi(4415)}. \qquad (18)$$
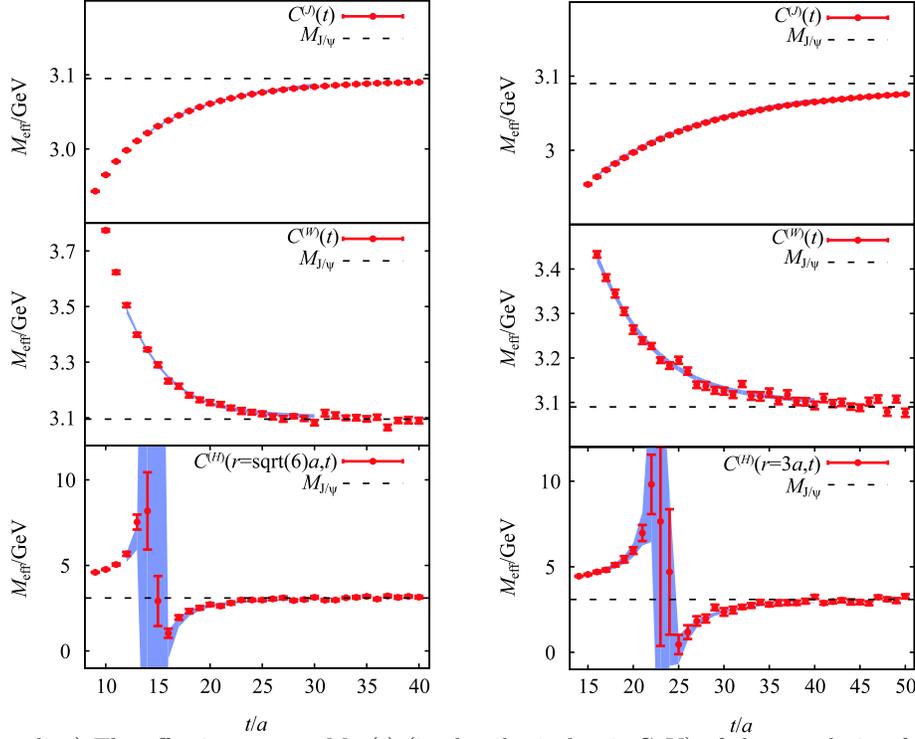

Fig. 4.   (color online) The effective masses $M_{\mathrm{eff}}(t)$ (in the physical unit GeV) of the correlation functions $C^{(X)}(t)$ with X standing for J, H, and W, respectively. The mass of the ground state (J/ψ) is plotted as a horizontal line to guide the eye. We also show the effective masses (in blue bands) of the functions in Eq. (12) using the fitted parameters at $t_{\min} = 12a_{\mathrm{t}}$ for $\beta = 2.4$ and $t_{\min} = 16a_{\mathrm{t}}$ for $\beta = 2.8$.

Table 2.   The spectral weights of the three states at different $t_{\min}$ on both lattices through a correlated three-mass-term fit. The errors are obtained through a jackknife analysis. The experimental results are also listed for comparison.

β	$t_{\min}$	$|Z_1^{(J)}Z_1^{(W)}|$	$|Z_2^{(J)}Z_2^{(W)}|$	$|Z_3^{(J)}Z_3^{(W)}|$	$|Z_1^{(W)}|^2$ $(\times 10^5)$	$|Z_2^{(W)}|^2$ $(\times 10^5)$	$|Z_3^{(W)}|^2$ $(\times 10^6)$
	11	14.3(0.6)	9.7(0.3)	1.3(1.9)	0.144(6)	0.08(5)	0.41(8)
	12	14.4(0.8)	9.5(0.5)	2.0(2.7)	0.146(7)	0.06(7)	0.33(9)
2.4	13	13.9(0.4)	9.9(0.7)	0.1(3.2)	0.142(3)	0.12(5)	0.39(17)
	14	13.8(0.4)	10.6(1.8)	3.3(7.2)	0.141(3)	0.15(9)	0.39(24)
	15	13.6(0.4)	11.6(2.5)	8.0(8.7)	0.140(2)	0.18(8)	0.33(24)
	14	33.6(2.8)	22.6(1.9)	0.3(2.1)	3.86(27)	0.88(0.97)	5.9(1.0)
	15	31.8(2.2)	21.6(1.1)	1.7(3.0)	3.65(22)	1.39(1.28)	4.3(1.1)
2.8	16	32.1(1.6)	21.5(0.9)	1.3(2.3)	3.68(14)	1.39(0.69)	3.9(0.7)
	17	33.1(4.0)	22.0(1.6)	0.0(5.2)	3.81(38)	0.66(1.95)	3.4(0.9)
	18	31.5(2.0)	20.7(1.1)	0.4(6.1)	3.64(15)	1.95(0.91)	7.7(2.9)

Table 3.   The masses and the leptonic decay constants of the three states at different $t_{\min}$ on both lattices. All the values are in GeV using the lattice spacings listed in Table 1. The errors are obtained through a jackknife analysis. The experimental results are also listed for comparison.

β	$t_{\min}$	$m_{\mathrm{J}/\psi}$	$f_{\mathrm{J}/\psi}$	$m_{\psi'}$	$f_{\psi'}$	m_3	f_3
	11	3.101(6)	0.47(2)	3.60(7)	0.4(1)	4.6(1)	-0.005(8)
	12	3.100(7)	0.47(2)	3.58(9)	0.4(2)	4.6(2)	-0.009(10)
2.4	13	3.097(4)	0.46(1)	3.64(6)	0.31(6)	4.7(2)	0.00(1)
	14	3.096(4)	0.46(1)	3.68(9)	0.29(6)	4.7(3)	0.01(3)
	15	3.095(4)	0.46(1)	3.72(9)	0.29(5)	4.7(3)	0.04(4)
	14	3.096(10)	0.44(2)	3.51(7)	0.5(4)	4.7(1)	0.001(5)
	15	3.090(9)	0.43(2)	3.56(8)	0.4(2)	4.6(2)	0.005(7)
2.8	16	3.090(6)	0.43(1)	3.54(5)	0.4(1)	4.6(1)	0.004(6)
	17	3.090(10)	0.43(3)	3.50(10)	0.6(8)	4.5(2)	0.00(2)
	18	3.088(8)	0.42(2)	3.55(7)	0.3(9)	4.9(2)	0.01(1)
	Expt.	3.097	0.407(5)	3.686	0.290(2)		

Since $|Z_3^{(W)}|^2 \gg |Z_1^{(W)}|^2 \sim |Z_2^{(W)}|^2$, we can take the approximation $Z_3^{(W)} \approx Z_{\mathrm{X}}^{(W)}$. Furthermore, if we assume $|Z_{\psi(4415)}^{(W)}| \sim |Z_2^{(W)}|$, from Table 2, we can take $Z_{\psi(4415)}^{(W)}/Z_{\mathrm{X}}^{(W)} \sim 1/5$. Using the experimental leptonic decay width of $\psi(4415)$, $\Gamma(\psi(4415) \to \mathrm{e}^+\mathrm{e}^-) = 0.58(7)$ keV, $f_{\psi(4415)}$ is extracted to be 157 MeV through the relation

$$\Gamma(\mathrm{V}_{c\bar{c}} \to \mathrm{e}^+\mathrm{e}^-) = \frac{16\pi}{27}\alpha_{\mathrm{QED}}^2 \frac{f_{\mathrm{V}}^2}{M_{\mathrm{V}}}, \qquad (19)$$

where we take $\alpha_{\mathrm{QED}} = 1/134$ at the charm quark mass scale. Therefore, f_{X} can be roughly estimated to be

$$f_{\mathrm{X}} \sim 30 \text{ MeV}. \qquad (20)$$

So we can assign a safer upper limit of f_{X} as

$$f_{\mathrm{X}} < \frac{1}{10}f_{\mathrm{J}/\psi} \sim 40 \text{ MeV}, \qquad (21)$$

which gives the upper limit of the leptonic decay width of the exotic vector charmonium,

$$\Gamma(\mathrm{X} \to \mathrm{e}^+\mathrm{e}^-) < 40 \text{ eV}. \qquad (22)$$

4   Discussion

The suprisingly small $\mathrm{e}^+\mathrm{e}^-$ decay width of the exotic vector charmonium X is in sharp contrast to that of conventional vector charmonia, which are usually of the order of keV. In other words, if this hybrid-like vector charmonium does exist in the real world, its contribution to the inclusive cross section of $\mathrm{e}^+\mathrm{e}^-$ annihilation is rather small. Actually the R value scan versus the invariant energy $\sqrt{s}$ of $\mathrm{e}^+\mathrm{e}^-$ collisions does not show any indication of an extra vector charmonium-like state around $\sqrt{s} = 4.3$ GeV (there is however a small dip in this energy range). The BEPCII/BESIII in Beijing is now accumulating $\mathrm{e}^+\mathrm{e}^-$ collision data in this energy range and will hopefully give a more precise line shape of the R-value here to clarify the situation. On the other hand, as mentioned above, the vector charmonium state X(4260) was observed by several experiments in the initial state radiation of $\mathrm{e}^+\mathrm{e}^-$ annihilation into $\mathrm{J}/\psi\pi^+\pi^-$. The combined decay width of X(4260) is

$$\Gamma(\mathrm{X}(4260) \to \mathrm{e}^+\mathrm{e}^-)Br(\mathrm{X}(4260) \to \mathrm{J}/\psi\pi\pi) = 9.2 \pm 1.0\,\mathrm{eV}. \qquad (23)$$

If X(4260) is tentatively assigned to the X state investigated in this study, combining the above value with the leptonic decay width of X, we can give an estimate of the branching ratio of X(4260) decaying into $\mathrm{J}/\psi\pi^+\pi^-$

$$Br(\mathrm{X}(4260) \to \mathrm{J}/\psi\pi\pi) > 20\%, \qquad (24)$$

which means that $\mathrm{J}/\psi\pi\pi$ is one of the most important decay modes of X(4260). This can naturally explain why X(4260) has only been observed in this channel to date. Furthermore, given the likely hybrid nature of the X state, it can be expected that the spin singlet $c\bar{c}$ component of X prefers a hadronic transition into spin singlet charmonium, such as h_c. So X(4260) $\to \mathrm{h}_c\pi\pi$ can also be an important decay mode of X(4260). Recently the BESIII Collaboration studied the $\mathrm{e}^+\mathrm{e}^- \to \pi^+\pi^-\mathrm{h}_c$ process at center-of-mass energies from 3.90 GeV to 4.42 GeV. They found that the cross sections are of the same order of magnitude as, but have different line shapes from, those of $\mathrm{e}^+\mathrm{e}^- \to \pi^+\pi^-\mathrm{J}/\psi$ [30]. It is highly desirable to investigate whether they are from the same resonance structure or not.

The reason for the large branching ratio of X(4260) $\to$ $\mathrm{J}/\psi\pi\pi$ can be depicted as follows. In the $\mathrm{e}^+\mathrm{e}^-$ annihilation, the charm quark-antiquark pair $c\bar{c}$ is produced in the short range through the virtual photon. During the hadronization procedure, the charm quark and the charm antiquark emit soft gluons continuously, which form a colored gluon halo around the gradually localized color octet $c\bar{c}$ (in a relative sense). Finally a meta-stable state is formed as the X(4260) particle. Obviously, the color octet $c\bar{c}$ kernel can be readily neutralized into a color singlet charmonium by absorbing (emitting) soft gluons from (to) the halo, and the gluon halo thereby becomes

color neutral and are emitted as light hadrons, for example, the $\pi\pi$ pair. If this is actually the case, the color flux between the charm quark and antiquark have less chance to be excited to a high enough energy to break, and thus the possibility of the $D\bar{D}$ decay modes are suppressed. There is a little similarity between this 'halo charmonium' picture and the so-called 'hadro-charmonium' picture, where the relatively localized color neutral $c\bar{c}$ kernel is surrounded by a light hadron cloud [31]. However, the advantage of the former is that the direct color interaction between the halo and the kernel provides an obvious binding mechanism, while in the 'hadro-charmonium' picture, more phenomenological assumptions are needed to describe the interaction between the meson cloud and the charmonium kernel.

5   Conclusion

To summarize, we use a new type of spatially extended hybrid-like operator to investigate the possible existence of exotic vector charmonia. In the nonrelativistic approximation of these operators, the localized color octet charm quark-antiquark component is in the spin singlet state and separates from the chromo-magnetic field strength with a spatial distance. These operators couple preferentially to a higher vector state

X with a mass of 4.33(2) GeV when the distance increases. This observation indicates that the charm quark-antiquark pair of X may acquire a center-of-mass motion by recoiling against additional degrees of freedom depicted by the chromo-magnetic field strength operators, which are necessarily gluonic in the quenched approximation. In this meaning, the state X can be taken as a hybrid-like vector charmonium. In addition, through a simultaneous multi-state fit to different correlation functions built from the vector current operator and the the hybrid operator mentioned above, the leptonic decay constant of X is tentatively determined to be roughly one order of magnitude smaller than $f_{J/\psi}$, say, $f_X < 40$ MeV, which gives a very small leptonic decay width $\Gamma(X \to e^+e^-) < 40$ eV. This is a very important characteristic parameter for X to be identified from experiments. Obviously the mass and the leptonic decay width of X are consistent with the production and decay properties of X(4260), which had so far escaped direct measurement in e^+e^- annihilation. Based on the combined width $\Gamma_{ee}\Gamma_{J/\psi\pi^+\pi^-}\Gamma_{tot} = 9.2\pm1.0$ eV of X(4260), if it can be assigned to the X state in this study, its decay branch fraction of $J/\psi\pi\pi$ mode can be larger than 20%, which also naturally explains why X(4260) is dominantly observed in $J/\psi\pi\pi$. By virtue of the inner structure of X, X(4260) should also be observed in the $h_c\pi\pi$ channel.

References

1   B. Aubert et al (BaBar Collaboration), Phys. Rev. Lett., **95**: 142001 (2005) [hep-ex/0506081]

2   C. Z. Yuan et al (Belle Collaboration), Phys. Rev. Lett., **99**: 182004 (2007) [arXiv:0707.2541 [hep-ex]]

3   T. E. Coan et al (CLEO Collaboration), Phys. Rev. Lett., **96**: 162003 (2006) [hep-ex/0602034]

4   K. A. Olive et al(Particle Data Group Collaboration), Chin. Phys. C, **38**: 090001 (2014)

5   S. L. Zhu, Phys. Lett., B **625**: 212 (2005) [hep-ph/0507025]

6   F. E. Close and P. R. Page, Phys. Lett., B **628**: 215 (2005) [hep-ph/0507199]

7   E. Kou and O. Pene, Phys. Lett., B **631**: 164 (2005) [hep-ph/0507119]

8   P. Lacock et al (UKQCD Collaboration), Phys. Rev. D, **54**: 6997 (1996) [hep-lat/9605025]

9   C. W. Bernard et al (MILC Collaboration), Phys. Rev. D, **56**: 7039 (1997) [hep-lat/9707008]

10   X. Liao and T. Manke, hep-lat/0210030

11   C. Bernard et al, Phys. Rev. D, **68**: 074505 (2003) [hep-lat/0301024]

12   Z. H. Mei and X. Q. Luo, Int. J. Mod. Phys. A, **18**: 5713 (2003) [hep-lat/0206012]

13   J. J. Dudek, R. G. Edwards, M. J. Peardon, D. G. Richards and C. E. Thomas, Phys. Rev. Lett., **103**: 262001 (2009) [arXiv:0909.0200 [hep-ph]]

14   L. Liu et al (Hadron Spectrum Collaboration), JHEP, **1207**: 126 (2012) [arXiv:1204.5425 [hep-ph]]

15   Y. B. Yang, Y. Chen, G. Li and K. F. Liu, Phys. Rev. D, **86**: 094511 (2012) [arXiv:1202.2205 [hep-ph]]

16   J. J. Dudek and E. Rrapaj, Phys. Rev. D, **78**: 094504 (2008)

[arXiv:0809.2582 [hep-ph]]

17   J. J. Dudek, R. Edwards and C. E. Thomas, Phys. Rev. D, **79**: 094504 (2009) [arXiv:0902.2241 [hep-ph]]

18   M. Berwein, N. Brambilla, J. Tarrús Castellà and A. Vairo, Phys. Rev. D, **92**: 114019 (2015) [arXiv:1510.04299 [hep-ph]]

19   L.L Foldy and S.A. Wouthuysen, Phys. Rev., **78**: 29 (1950); S. Tani, Prog. Theor. Phys., **6**: 267 (1951)

20   C. J. Morningstar and M. J. Peardon, Phys. Rev. D, **56**: 4043 (1997) [hep-lat/9704011]

21   C. J. Morningstar and M. J. Peardon, Phys. Rev. D, **60**: 034509 (1999) [hep-lat/9901004]

22   Y. Chen et al, Phys. Rev. D, **73**: 014516 (2006) 014516 [hep-lat/0510074]

23   C. Liu, J. h. Zhang, Y. Chen and J. P. Ma, Nucl. Phys. B, **624**: 360 (2002) [hep-lat/0109020]

24   L. M. Liu, S. q. Su, X. Li and C. Liu, Chin. Phys. Lett., **22**: 2198 (2005) [hep-lat/0505006]

25   Y. B. Yang et al (CLQCD Collaboration), Phys. Rev. D, **87**: 014501 (2013) [arXiv:1206.2086 [hep-lat]]

26   G. T. Bodwin, E. Braaten and G. P. Lepage, Phys. Rev. D, **51**: 1125 (1995); Erratum: Phys. Rev. D, **55**: 5853 (1997) [hep-ph/9407339]

27   Y. Chen et al (CLQCD Collaboration), hep-lat/0701021

28   J. J. Dudek, R. G. Edwards and D. G. Richards, Phys. Rev. D, **73**: 074507 (2006) [hep-ph/0601137]

29   L. C. Gui et al (CLQCD Collaboration), Phys. Rev. Lett., **110**: 021601 (2013) [arXiv:1206.0125 [hep-lat]]

30   M. Ablikim et al (BESIII Collaboration), Phys. Rev. Lett., **111**: 242001 (2013) [arXiv:1309.1896 [hep-ex]]

31   S. Dubynskiy and M. B. Voloshin, Phys. Lett. B, **666**: 344 (2008) [arXiv:0803.2224 [hep-ph]]